Primary and secondary dissociation pathways in the ultraviolet photolysis of Cl_2O

Christine M. Nelson, Teresa A. Moore, and Mitchio Okumura[a)]
Arthur Amos Noyes Laboratory of Chemical Physics,[b)] California Institute of Technology, Pasadena, California 91125

Timothy K. Minton[a)]
Jet Propulsion Laboratory, California Institute of Technology, Pasadena, California 91109

(Received 9 December 1993; accepted 24 February 1994)

The photodissociation of dichlorine monoxide (Cl_2O) at 308, 248, and 193 nm was studied by photofragment translational energy spectroscopy. The primary channel upon excitation at 308 and 248 nm was Cl–O bond fission with production of ClO+Cl. A fraction of the ClO photoproducts also underwent spontaneous secondary dissociation at 248 nm. The center-of-mass translational energy distribution for the ClO+Cl channel at 248 nm appeared to be bimodal with a high energy component that was similar in shape to the 308 nm distribution and a second, low energy component with a maximum close to the threshold for the $2Cl+O(^3P)$ channel. Observation of a bimodal distribution suggests that two pathways with different dissociation dynamics lead to ClO+Cl products. The high product internal energy of the second component raises the possibility that ClO is formed in a previously unobserved spin-excited state $a\,^4\Sigma^-$. Following excitation at 193 nm, a concerted dissociation pathway leading to Cl_2+O was observed in addition to primary Cl–O bond breakage. In both processes, most of the diatomic photofragments were formed with sufficient internal energy that they spontaneously dissociated. The time-of-flight distributions of the Cl_2+O products suggest that these fragments are formed in two different channels $Cl_2(^3\Pi)+O(^3P)$ and $Cl_2(X\,^1\Sigma)+O(^1D)$.

I. INTRODUCTION

The importance of chlorine-catalyzed ozone loss cycles in the stratosphere has motivated studies of the photochemistry of chlorine-containing compounds. Among the chlorine oxides, dichlorine monoxide (Cl_2O, also referred to as chlorine monoxide) is currently thought to play a minor role in stratospheric chemistry. However, a study of its photochemistry can deepen our understanding of the photochemistry of related molecules; furthermore, Cl_2O is frequently used in laboratory studies of chlorine/oxygen chemistry, in flow tube studies as a photolytic precursor for ClO, and in molecular beam studies to calibrate the relative detector sensitivity for Cl and ClO fragments. Correct interpretation of such experiments requires characterization of Cl_2O photochemistry, but the photodecomposition pathways are still uncertain, especially at shorter wavelengths ($\lambda<300$ nm).

Cl_2O possesses a complex manifold of electronically excited states. The four highest filled molecular orbitals of Cl_2O are nearly degenerate nonbonding and weakly antibonding orbitals, and excitation of electrons from these orbitals gives rise to several transitions in the visible and ultraviolet. The absorption spectrum contains overlapping continuous bands between 660 and 220 nm. The most prominent of those features are a maximum at 255 nm and a shoulder at 280 nm (see Fig. 1).[1] Two additional strong features appear in the vacuum ultraviolet, a strong continuous band with a peak at 171.3 nm (whose onset at 220 nm can be seen in Fig. 1) and a structured Rydberg transition with an origin at 162.9 nm.[2]

Earlier experiments on the UV photochemistry of Cl_2O involved the measurement of the final product quantum yields at high reactant pressures and the determination of the chain propagation mechanisms. Finkelnburg *et al.*[3] investigated both the direct and chlorine-sensitized photochemical decompositions of Cl_2O at 313, 365, and 436 nm. From an observed final Cl_2 product quantum yield of 3.5, they deduced that[4]

$$Cl_2O+h\nu\rightarrow ClO+Cl, \quad \Delta H_0^\circ=32.9 \text{ kcal/mol} \qquad (1)$$

was the initial Cl_2O decomposition step. Several studies later suggested that atomic oxygen is produced directly from Cl_2O by photolysis at shorter wavelengths

$$Cl_2O+h\nu\rightarrow 2Cl+O(^3P), \quad \Delta H_0^\circ=96.4 \text{ kcal/mol}, \qquad (2)$$

$$Cl_2O+h\nu\rightarrow Cl_2+O(^3P), \quad \Delta H_0^\circ=39.2 \text{ kcal/mol}. \qquad (3)$$

Schumacher and Townend[5] observed an increased quantum yield of 4.5 upon irradiation in the wavelength range 235–275 nm. They proposed that channel (2) was the only Cl_2O dissociation pathway occurring below 275 nm. To explain the unit increase in quantum yield at shorter wavelengths, they had to assume that oxygen atoms do not react with ClO; however, subsequent experiments have shown that the $O+Cl_2O$ reaction is fast.[6] Edgecomb *et al.* reexamined Cl_2O photochemistry by flash photolysis at $\lambda>281$ nm and direct detection of ClO intermediates.[7] They suggested that the increased quantum yield observed by Schumacher and Townend was due to limited initial formation of O atoms by reaction (2), followed by rapid reaction of these atoms with

a)Authors to whom correspondence should be addressed.
b)Contribution number 8901.

 0021-9606/94/100(11)/8055/10/$6.00

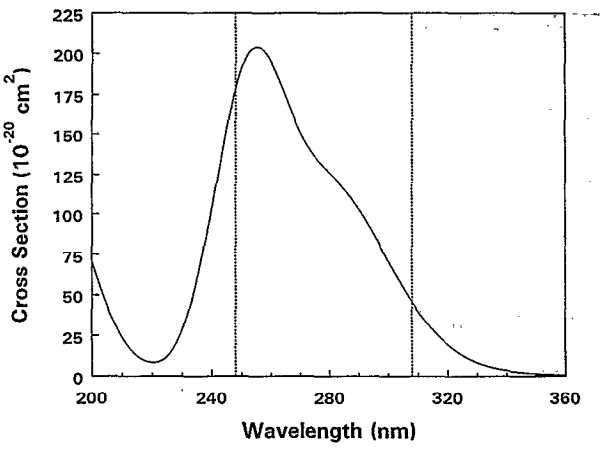

FIG. 1. The absorption spectrum of Cl_2O. Points are taken from Ref. 17 based on an evaluation of published spectra in Ref. 1.

Cl_2O. In a more recent flash-photolysis study, Basco and Dogra found an average final product quantum yield of Cl_2 of 4.9 ± 1.0 at all wavelengths, regardless of the presence of Cl_2.[8] When they photolyzed Cl_2O at $\lambda<310$ nm, they also observed vibrationally excited oxygen O_2^*, which they conjectured could only be formed by reactions of atomic oxygen

$$O+Cl_2O\rightarrow 2Cl+O_2^*, \tag{4}$$

$$O+ClO\rightarrow Cl+O_2^*. \tag{5}$$

They inferred that there were two possible sources of oxygen atoms—photolysis of Cl_2O and photolysis of ClO. Their data was most consistent with O atoms formed entirely by secondary photodissociation of the primary ClO products

$$ClO+h\nu\rightarrow Cl+O. \tag{6}$$

They concluded that no compelling case could be made for atomic oxygen produced directly from photolysis of Cl_2O. Prior to 1989, there was thus conflicting evidence for reaction (2) or reaction (3). All of these earlier studies relied on indirect detection of O atoms and an incomplete understanding of the reaction kinetics, especially of the ClO self-reaction.

Sander and Friedl used Cl_2O photolysis to form ClO in a recent flow tube study of the BrO+ClO reaction.[9] When they photolyzed Cl_2O with broadband radiation from a xenon flashlamp ($\lambda>180$ nm through quartz) in the presence of Br_2, they detected BrO products as well. BrO could only be produced by the reaction

$$O+Br_2\rightarrow BrO+Br. \tag{7}$$

They concluded that atomic oxygen was formed directly from Cl_2O photolysis by either reaction (2) or reaction (3). From the BrO yield, they obtained an O atom quantum yield of 0.25 ± 0.05 integrated over the intensity distribution of the flashlamp. They could not measure the wavelength dependence of the quantum yield, nor could they identify the specific Cl_2O dissociation channels leading to O atom production.

The primary and secondary channels in the photodissociation of Cl_2O can be probed and differentiated by the technique of photofragment translational energy spectroscopy, which allows the direct detection of photoproducts and the determination of their translational energy and angular distributions. We have employed this method to study the UV photodissociation of dichlorine monoxide. In an earlier communication,[10] we used the photolysis of Cl_2O at 308 nm to calibrate the relative detection efficiencies of our mass spectrometer for Cl and ClO photofragments. In this paper, we present full results of the study of dichlorine monoxide photolysis at 308 and 248 nm, as well as preliminary data at 193 nm. The ClO+Cl and $Cl_2+O(^3P)$ channels are energetically accessible at all three wavelengths, but the $Cl+Cl+O(^3P)$ channel can only be reached at 193 and 248 nm. By photolyzing Cl_2O at these wavelengths, we can compare the dissociation dynamics upon excitation to different regions of the Cl_2O absorption spectrum.

II. EXPERIMENT

The experimental apparatus and methods are described in detail elsewhere,[11] and only a brief outline is presented here. A continuous molecular beam of Cl_2O was formed by passing helium over the surface of liquid Cl_2O (vapor pressure of 6.9 Torr at -74 °C) and expanding the mixture through a 0.1 mm diameter water-cooled glass nozzle (4.9 °C) at a total stagnation pressure of 200 Torr. A skimmer confined the beam to an angular divergence of 3.4°. A rectangular slit aperture further collimated the beam to a 2.3 mm×3.0 mm spot in the interaction region. The nozzle was 4.8 cm from the interaction volume, where the molecular beam intersected the focused, unpolarized beam of a pulsed excimer laser. The density of Cl_2O in the interaction volume was approximately 10^{11} cm^{-3}. After a laser pulse, the resulting photoproducts scattered out of the interaction region and were detected off the beam axis with a mass spectrometer rotatable in the plane of the molecular beam and laser. The distance from the photolysis volume to the Brinks ionizer of the mass spectrometer was 34.1 cm. Time-of-flight (TOF) spectra of the fragments were recorded with a multichannel scaler in 2 μs steps. Electron energies in the ionizer were nominally 160 eV (set by optimizing ion signal), but the actual energy was lower due to space-charge effects at the emission currents used in these experiments. The velocity distribution of the parent molecular beam was determined by chopping the beam with a slotted disk and measuring the TOF distribution with the detector positioned on the beam axis. The correction for the flight time of ions from the ionizer to the Daly detector was found to be $t=3.54\ (m/e)^{1/2}$ μs.

Cl_2O synthesis followed techniques presented in the literature.[12] The main impurity, Cl_2, was removed by pumping on the sample at -118 °C (ethanol slush bath). Running the molecular beam prior to performing the experiment served as a further purification step by preferentially removing the more volatile Cl_2. After the molecular beam velocity had stabilized, data collection proceeded.

A Lambda Physik EMG 101 excimer laser was used to provide the excitation wavelengths of 193, 248, or 308 nm.

Pulse energies in the interaction region were 13–25, 48–60, or 9–22 mJ and spot sizes were (width by height) 2.3×3.5, 4.7×2.4, or 3.3×1.4 mm, respectively. We measured the fluence dependence of the $m/e=35$ TOF spectra at all wavelengths in order to identify and minimize contributions from stimulated secondary dissociation of primary ClO photofragments. The laser pulse energy was attenuated to the levels quoted above with quartz plates until the shape of the $m/e=35$ TOF spectra no longer varied with intensity.

TOF spectra were recorded at $m/e=35$ (Cl^+), 51 (ClO^+), 70 (Cl_2^+), and 16 (O^+) and at detector angles from 10° to 60°. Each TOF spectrum was averaged for 100 000 to 500 000 laser pulses. Angular distributions at 248 and 308 nm were recorded at $m/e=51$ over the range 10°–50°. The 248 nm distribution was made in 10° increments with four scans of 10 000 laser pulses each for a total of 40 000 laser pulses at each angle. The 308 nm distribution was recorded in 5° increments with six scans for a total of 60 000 laser pulses at each angle. The angular distribution of the $m/e=16$ signal from 193 nm photolysis was measured from 10° to 60° in two scans for a total of 20 000 shots at each angle.

III. RESULTS AND ANALYSIS

Fragments recoiling upon dissociation can be characterized by a center-of-mass (c.m.) translational energy distribution $P(E_T)$ and a c.m. angular distribution $w(\theta)\propto 1+\beta P_2(\cos\theta)$, where E_T is the total c.m. translational energy of the products, θ is the angle between the electric field vector of the radiation and the relative product velocity (recoil) vector, and P_2 is the second Legendre polynomial.[13] The available energy $E_{avl}=h\nu-\Delta H_0^\circ$, is partitioned between the c.m. translational energy E_T and fragment internal energy E_{int}. The anisotropy parameter β, which is determined by the angle between the transition moment and recoil vector, varies from 2 (parallel) to −1 (perpendicular). If the dissociation is not instantaneous, the molecule will have time to rotate. Even partial averaging over molecular orientations by rotation reduces the observed anisotropy and diminishes the value of β.[14] For linear molecules with lifetimes greater than a rotational period, β is reduced by a factor of 4; for polyatomics, β can approach zero. The TOF spectra are measured in the laboratory (LAB) frame at fixed detector angles. The $P(E_T)$ and $w(\theta)$ distributions are related to velocity and angular distributions in the LAB frame by a c.m.-to-LAB coordinate transformation, with intensities scaled by the appropriate Jacobian determinant.[15] In analyzing the data for a given channel, we seek to find the c.m. distributions which best fit the observed TOF spectra at all laboratory angles.

We determine the anisotropy parameter β for each primary channel by fitting the recorded angular distribution. Each TOF spectrum is then fit by a forward convolution method[15] in which a trial numerical c.m. translational energy distribution is convoluted with experimental parameters and the c.m. angular distribution, and then transformed into a TOF spectrum in the LAB frame. This procedure is repeated with the $P(E_T)$ function and β parameter iteratively adjusted until the TOF spectra predicted by a single $P(E_T)$ distribution satisfactorily fit the data at all angles. We have not attempted to model the secondary dissociation of the primary photofragments in the current analysis.

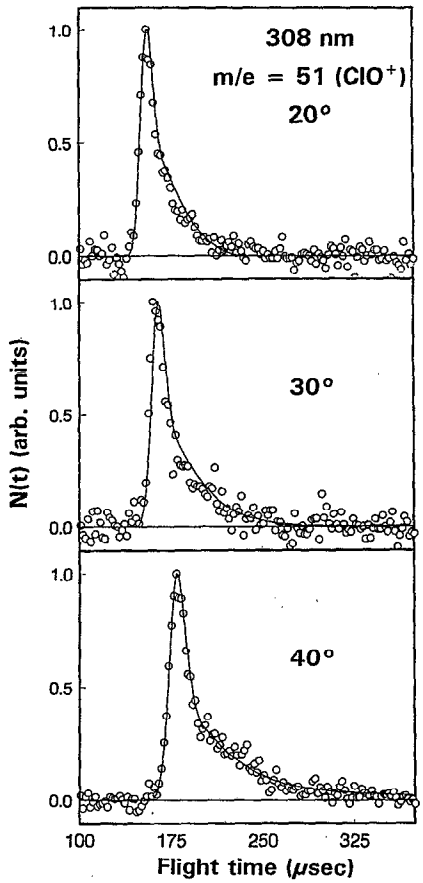

FIG. 2. Laboratory TOF distributions of $m/e=51$ at 308 nm for three detector angles. The solid lines are the best fits.

In many cases, we recorded TOF spectra for both products from a primary two body dissociation channel and could therefore exploit the conservation of linear momentum to confirm our assignment. The two fragments recoil with equal and opposite momenta in the c.m. frame of reference, and the TOF spectra of both products are described by the same c.m. translational energy $P(E_T)$ and angular $w(\theta)$ distributions. We could thus use the c.m. distribution obtained by fitting the TOF spectra of one product to predict that of its counterfragment.

A. 308 nm

We observed photoproduct signals at $m/e=16$, 35, and 51 from the photolysis of Cl_2O at 308 nm. The $m/e=51$ (ClO^+) TOF spectra, shown in Fig. 2 for various laboratory angles, consisted of a sharp peak with a slow tail. These products had an anisotropic angular distribution that was fit with $\beta=0.5$. With the exclusion of cluster dissociation, the only plausible assignment for the $m/e=51$ signal is ClO formed in channel (1). The $P(E_T)$ distribution that fit the ClO^+ spectra is displayed in the upper panel of Fig. 3.

In the $m/e=35$ TOF spectra shown in Fig. 4, two peaks

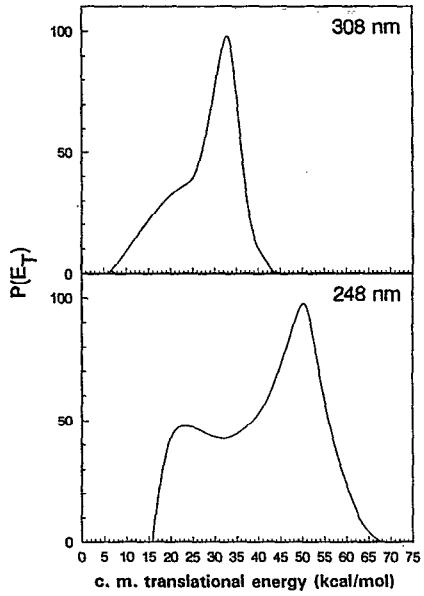

FIG. 3. The c.m. translational energy distributions $P(E_T)$ for the ClO+Cl channel at 308 (upper) and 248 nm (lower) determined by fitting the m/e =51 TOF spectra at the respective wavelengths.

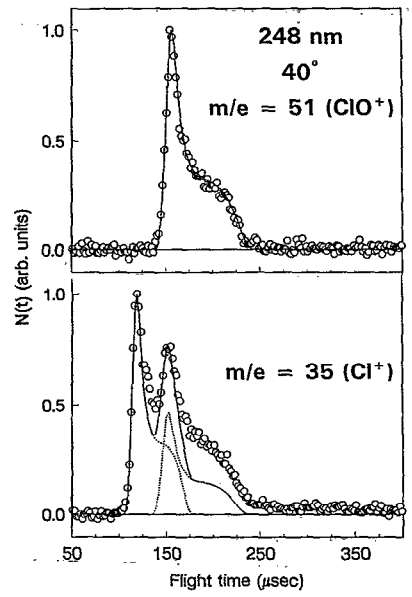

FIG. 5. Laboratory TOF distributions of m/e=51 and m/e=35 at 248 nm for a 40° detector angle. The solid lines are the calculated fits using the $P(E_T)$ distribution shown in Fig. 3. The dashed lines in the m/e=35 TOF spectrum are the contributions from each product.

were apparent. The shape of the slower peak was identical to the m/e=51 peak after correcting for the difference between the m/e=35 and 51 ion flight times; therefore, we attributed this slower peak to cracking of ClO products in the ionizer to form Cl^+. We assigned the fast, sharp peak to the Cl counterfragment. To confirm these assignments, we used the $P(E_T)$ distribution and β parameter derived from the ClO analysis to fit the TOF spectra at m/e=35. Cl is formed in the same dissociation event as ClO, so a fit to each component at m/e=35 can be calculated with the respective c.m.-to-LAB transformation of the same $P(E_T)$ distribution. A complete fit of the TOF spectrum requires only one adjustable parameter, the relative scaling factor of the two components. The agreement between the predicted and observed TOF spectra shown in Fig. 4 verifies that the two components arise from the momentum-matched counterfragments formed in the ClO+Cl channel and eliminates the possibility that the fragments were produced from the photodissociation of clusters. Given the success of the fit and the absence of signal at m/e=70, we conclude that only the ClO+Cl channel is observed when photolyzing Cl_2O at 308 nm.

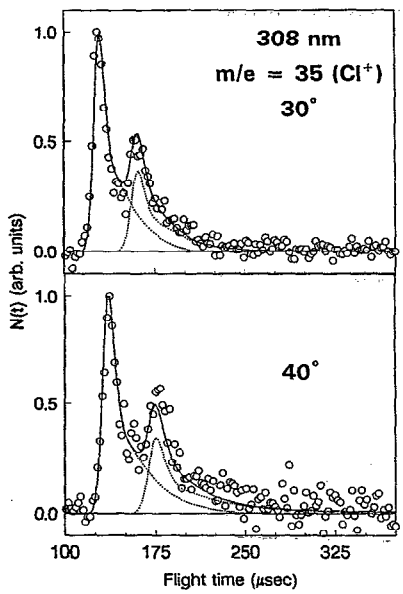

FIG. 4. Laboratory TOF distributions of m/e=35 at 308 nm for two detector angles. The solid lines are the calculated fits using the $P(E_T)$ distribution shown in the lower panel of Fig. 3. The dashed lines are the individual contributions from the Cl and ClO fragments.

B. 248 nm

The products detected at 248 nm exhibited TOF distributions (Fig. 5) similar to those obtained at 308 nm. The m/e=51 spectra each had a single peak with a pronounced shoulder, while the m/e=35 spectra consisted of two peaks, the slower one identified as an ionizer crack of the product detected at m/e=51. We again fit the m/e=51 TOF spectra assuming that the signal came entirely from primary ClO products arising from the ClO+Cl channel. A fit of the m/e =51 angular distribution gave β=0.5. The $P(E_T)$ distribution (see the lower panel of Fig. 3) and β parameter were then used to predict the m/e=35 TOF spectra (see Fig. 5). The predicted spectra matched the two main peaks observed in the m/e=35 spectra, although they do not account for all of the signal detected at m/e=35. The ClO+Cl channel must be a major photodissociation channel at 248 nm, but it is not the only dissociation pathway.

The discrepancy between the predicted and observed TOF spectra at m/e=35 appears as a broad background be-

neath the ClO peak, suggesting that secondary Cl atom products are formed by spontaneous dissociation of primary ClO fragments. The available energy at 248 nm is 82 kcal/mol, sufficient for secondary dissociation of ClO (D_0=63.4 kcal/mol). We observe a significant probability for ClO products formed near the dissociation limit, and formation of ClO with sufficient energy to dissociate is thus plausible.

Secondary photodissociation of the ClO photofragments[16]

$$ClO+h\nu \rightarrow Cl+O(^1D) \qquad (3')$$

is also a possible source of atomic chlorine, because the absorption cross section of ClO at 248 nm is $\sigma_{ClO}=3.2\times10^{-18}$ cm^2, almost twice that of Cl_2O ($\sigma_{Cl_2O}=1.7\times10^{-18}$ cm^2).[17] We were able to identify products from photolysis of ClO by examining the power dependence of the signal at $m/e=35$. At high laser fluences, new peaks appear that are forward and backward scattered from the primary ClO signal at $m/e=35$, the result of photodissociation of the ClO fragments. These peaks are absent in the TOF spectra used in the data analysis, which were collected at reduced laser fluence. Stimulated secondary dissociation of ClO therefore does not contribute appreciably to the Cl atom signal seen in Fig. 5.

The $P(E_T)$ distribution derived from $m/e=51$ provides information only on the channel leading to ClO products stable enough to reach the detector. A complete $P(E_T)$ distribution could in principle be extracted from the TOF spectrum of the primary Cl atom fragment, but the slow tail of the primary distribution overlaps the secondary Cl atom signal, and these contributions could not be deconvoluted. The $P(E_T)$ distribution shown in Fig. 3 (lower panel) is therefore truncated at low energies and does not include the contribution from ClO that had undergone secondary dissociation.

The $P(E_T)$ distribution extends to a low energy threshold of 16 kcal/mol. For products observed with total translational energy less than 19 kcal/mol, the internal energy exceeds the Cl–O bond dissociation energy.[18] There are a number of ways to account for the observation of intact ClO products that appear to have internal energies above the dissociation limit. First, there are uncertainties of 2 kcal/mol in the fit and 0.5 kcal/mol in the Cl_2O heat of formation. Second, energy could be partitioned into spin–orbit excitation of the Cl atom (the $^2P_{1/2}$ state, 2 kcal/mol), the ClO fragment (the $^2\Pi_{1/2}$ state, 1 kcal/mol), or both. Finally, ClO products could be metastable (bound by a centrifugal barrier) if formed in high rotational levels. The equilibrium bond angle is 110°, and in this geometry, a departing Cl atom would impart a large torque on the ClO fragment. With the use of either soft or rigid radical models,[19] we estimate that as much as 40%–50% of the available energy could be initially partitioned into ClO rotation. ClO radicals in such high J states would have centrifugal barriers supporting vibrational levels up to 6 kcal/mol above the Cl–O dissociation limit. Although some ClO products thus appear to be metastable with internal energies above the dissociation limit, the inability to fit the $m/e=35$ TOF distribution in the same way that the 308 nm TOF was fit implies that a fraction of the ClO products are formed so internally hot that they dissociate.

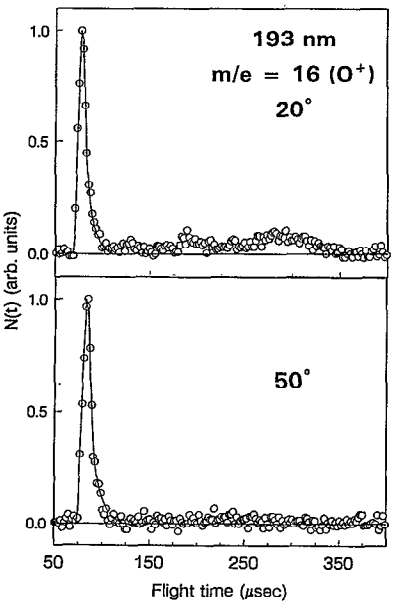

FIG. 6. Laboratory TOF distributions of $m/e=16$ at 193 nm for two detector angles. Circles are experimental points and the solid lines are the fits obtained using the $P(E_T)$ distribution for the Cl_2+O channel shown in Fig. 7.

C. 193 nm

The primary goal of our experiment was the study of Cl_2O photolysis at 308 and 248 nm. Our 193 nm study, while more exploratory, did reveal the main features of the dissociation dynamics at this wavelength.

The $m/e=16$ TOF spectra collected at 20° and 50° are shown in Fig. 6. The angular distribution at this mass was fit with an anisotropy parameter of $\beta=0.4$. We observed a prominent peak arriving at short times that was not detected at other masses, indicating that the signal probably arises from O atom products from the concerted dissociation $Cl_2O \rightarrow Cl_2+O$. From fits of the TOF spectra (solid lines in Fig. 6), we obtained the $P(E_T)$ distribution shown in Fig. 7. This distribution had a peak at E_T=42 kcal/mol and ended at E_T=56 kcal/mol, 4 kcal/mol above the threshold for the $2Cl+O(^3P)$ channel.

We tried to fit the TOF spectra of the counterfragment Cl_2 at $m/e=70$ using the $P(E_T)$ distribution and anisotropy parameter β obtained from fitting the O atom data. The TOF distribution predicted by the full $P(E_T)$ distribution (the dashed line in Fig. 8) fit only the leading edge of the observed $m/e=70$ TOF spectrum. The discrepancy was removed (solid line of Fig. 8) if the $P(E_T)$ distribution was truncated (the shaded area in Fig. 7) by assuming that Cl_2 fragments formed with internal energy greater than $D_0(Cl_2)$=57.2 kcal/mol dissociated before reaching the detector. From the difference between this truncated $P(E_T)$ distribution and the distribution obtained from the O atom data, we estimated that 87% of the Cl_2 products undergo secondary dissociation. The Cl_2 dissociation could only occur if the O atom counterfragments were in the ^3P state.

A secondary peak at $m/e=70$ occurred at $t=225$ μs in the TOF spectrum at 20° (see Fig. 8); products at these ve-

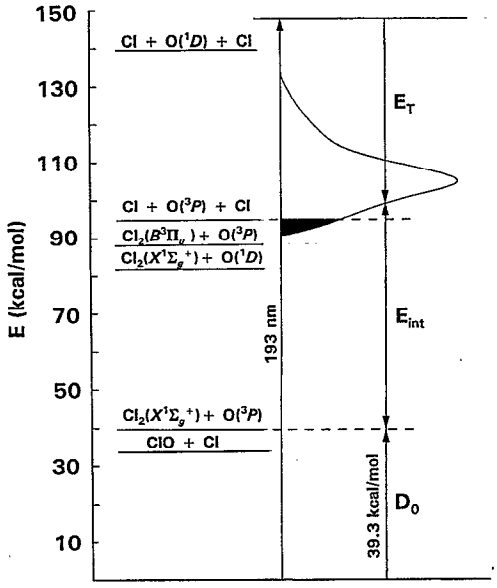

FIG. 7. The $P(E_T)$ distribution for the Cl_2+O channel upon photolysis at 193 nm derived from TOF spectra at m/e=16, plotted against an energy level diagram. The shaded area shows the translational energies which correspond to internal energies less than the Cl–Cl bond dissociation energy.

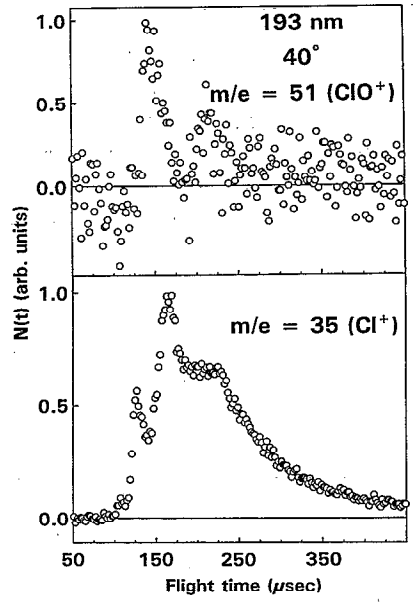

FIG. 9. Laboratory TOF distributions of m/e=51 and m/e=35 at 193 nm recorded at a 40° detector angle.

locities also contributed significantly to the slow peak observed at 30°. These Cl_2 products were momentum matched with O atom counterfragments in the low energy tail of the $P(E_T)$ distribution in Fig. 7. Fragments at the peak had E_T=19 kcal/mol, while those at the leading edge had E_T=30 kcal/mol, corresponding to E_{int}=79 kcal/mol. We thus observed Cl_2 signal well above the threshold for the $2Cl+O(^3P)$ channel. Bound Cl_2 could only be observed if the O atom was in an excited state. Therefore, we tentatively assign this signal to the pathway forming spin-excited oxygen atoms, the $Cl_2(X\ ^1\Sigma_g^+)+O(^1D)$ channel.

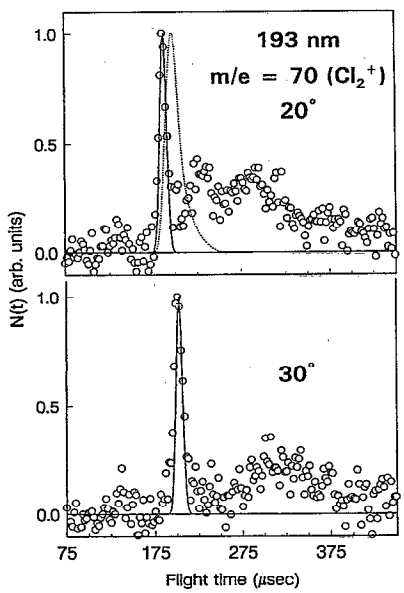

FIG. 8. Laboratory TOF distributions of m/e=70 at 193 nm for two detector angles. The dashed lines are the fits obtained using the full $P(E_T)$ distribution for the Cl_2+O channel (shown in Fig. 7) determined from the m/e=16 signal. The solid lines are the fits calculated using the $P(E_T)$ distribution truncated at $E_T \geq D_0(Cl_2)$.

We observed signal at still longer arrival times in the 20° TOF spectra at both m/e=70 and 16 (see Fig. 8). These peaks occurred at LAB velocities close to the parent beam velocity, indicating that the products were formed with little translational energy (E_T=2 and 8 kcal/mol at m/e=16 and 70, respectively, assuming the products are Cl_2+O from the Cl_2O monomer). The signal could arise from a number of channels, including cluster dissociation or, for the m/e=16 signal, secondary dissociation. The relatively low signal to noise ratio and lack of angular distribution information prevented further analysis.

The m/e=35 and 51 TOF spectra were recorded at 40° (Fig. 9). Although we were unable to extract a $P(E_T)$ distribution, correlations between the two TOF spectra provide strong evidence for the ClO+Cl channel. At m/e=51, a weak peak arriving at 152 μs was apparent. If we were to assign this peak to ClO products from the ClO+Cl channel, then E_T would be 54 kcal/mol, and the counterfragment Cl atoms would arrive at 110 μs, which corresponds to the fast signal in the m/e=35 TOF spectrum. In addition, the Cl atoms arriving at the leading edge (t=100 μs) of the m/e=35 TOF spectrum can be momentum matched with the fastest ClO at 130 μs with E_T=82 kcal/mol. The m/e=51 TOF spectrum fell off rapidly at $t \approx 155$ μs, coinciding with the onset for secondary dissociation of the ClO fragments, i.e., $E_{int} > D_0(ClO)$.

The TOF spectrum at m/e=35 consisted of a number of superimposed peaks (the lower panel of Fig. 9). Sources of m/e=35 signal include cracking of Cl_2 and ClO in the ionizer to form Cl^+, primary Cl photofragments formed via the Cl+ClO channel, atomic chlorine from spontaneous second-

ary dissociation of ClO and Cl_2, and possibly concerted three body decomposition to 2Cl+O. Extensive secondary dissociation was evident. The peak at 127 μs appears to arise from Cl photofragments that are momentum matched to ClO products that undergo spontaneous secondary dissociation and give rise to the strong $m/e=35$ peak at 165 μs.

Fragmentation to 2Cl+O appears to be a major channel in the photolysis of Cl_2O at 193 nm; however, we were unable to deconvolute the strongly overlapping velocity distributions from these secondary channels and thus could not measure the relative yields for the various channels. Atomic fragments could also arise from a concerted three body process, but we were unable to identify such a channel because of the complexity of the $m/e=35$ TOF spectrum and the difficulty in modeling three body dissociation dynamics.

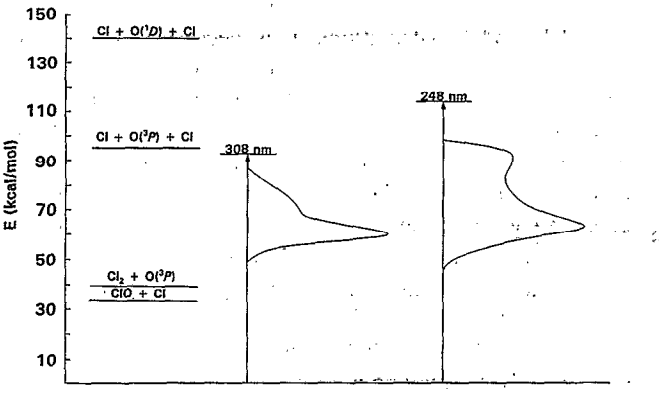

FIG. 10. The energy level diagram for the photodissociation of Cl_2O at 308 and 248 nm. The $P(E_T)$ distributions for ClO+Cl are shown to illustrate how the available energy is partitioned at the two wavelengths.

IV. DISCUSSION

A. ClO+Cl channel

We have observed simple Cl–O bond fission leading to ClO+Cl products at all three wavelengths. The ClO+Cl channel is the only dissociation channel following excitation at 308 nm, a major channel at 248 nm, and a minor channel at 193 nm. These findings agree with Finkelnburg *et al.*,[3] who concluded that above 300 nm, the only photodissociation pathway is ClO+Cl. Our results contradict the conclusion of Schumacher and Townend[5] that photolysis of Cl_2O from 235 to 275 nm produced only atomic fragments 2Cl+O.

The dissociation dynamics at 308 and 248 nm appear to be similar, having identical values for the β parameter and sharing common features in their $P(E_T)$ distributions. $\beta=0.5$ implies that the angle between the transition moment and the recoil velocity vector is $\leqslant 45°$. The transition dipole is thus approximately in plane and perpendicular to the C_{2v} symmetry (A_1) axis, indicating optical transitions to states of B_2 symmetry. If we assume that the geometry during dissociation is similar to that of the ground state, we calculate that complete rotational averaging will yield $\beta<0.19$.[14] From the observed anisotropy of the angular distributions and the large translational energy release, we conclude that dissociation occurs within a rotational period. The $P(E_T)$ distributions are plotted together in Fig. 10. Both distributions appear to have more than one component. The faster component in each distribution dominates, and both have peaks at $E_{\text{int}}\approx 30$ kcal/mol. The $P(E_T)$ distribution at 308 nm has a slow shoulder with a low energy cutoff at $E_T=6$ kcal/mol, corresponding to $E_{\text{int}}=54$ kcal/mol. The faster component of the 248 nm distribution is similar in shape to the 308 nm distribution and differs only at low E_T, where there is a second maximum at $E_T=23$ kcal/mol or $E_{\text{int}}=59$ kcal/mol. It is likely that the 248 nm distribution extends to lower translational energies (higher internal energies), where secondary dissociation of ClO occurs.

In contrast to the longer wavelength distributions, the ClO products from photolysis at 193 nm are only formed with high internal energies near and above the dissociation limit ($E_{\text{int}}\geqslant 33$ kcal/mol).

The observation of multiple components in the $P(E_T)$ distribution at 248 nm implies that different dissociation dynamics lead to the same final products ClO+Cl. The low-energy shoulder in the $P(E_T)$ distribution at 308 nm could also be interpreted as a second pathway, but such a conclusion is more tentative. Partially resolved vibrational structure could give the appearance of two components at 308 nm. The fast component in the 248 nm $P(E_T)$ distribution is similar to the 308 nm distribution (see Fig. 10) and thus may be attributable to the same dynamical pathway. The second peak at 248 nm could then be interpreted as products from a new dynamical pathway. On the other hand, the low energy shoulder at 308 nm could be the onset of a new channel which develops into the second peak at 248 nm as the photolysis wavelength decreases. These alternatives could be distinguished in a study of the wavelength dependence of the shape of the $P(E_T)$ distribution.

Bimodal distributions can arise if two or more potential energy surfaces are involved in the dissociation. The irregular shape of the absorption spectrum[1] between 220 and 600 nm suggests the presence of several electronic states. The strongest bands are at 255 and ~280 nm. It is thus possible to excite two repulsive states of Cl_2O, both of which lead to ClO+Cl products. We observe, however, that all components have the same anisotropy, within experimental error. This result is more consistent with excitation to a single electronic state of Cl_2O followed by a nonadiabatic transition to a second surface. In either case, different excited state surfaces leading to ClO+Cl products may correlate to different final spin–orbit states, but our time-of-flight resolution precludes us from distinguishing among the possible spin–orbit channels.

The bimodal distribution could also be explained if ClO products were formed in an electronically excited state. The report by Nee and Hsu[20] of resolved ClO fluorescence upon excitation of Cl_2O in the vacuum ultraviolet indicates that the ClO photoproduct is formed in several Rydberg states, from the C to the H states. These states are not accessible at the longer wavelengths used in this study. The lowest known excited state of ClO is the $A\ ^2\Pi$ state, but the channel

$$Cl_2O \rightarrow ClO(A\ ^2\Pi) + Cl(^2P_{3/2}), \quad \Delta H_0^\circ = 122 \text{ kcal/mol} \quad (8)$$

is also energetically inaccessible at 248 or 308 nm.

In order for electronic excitation to account for the observed bimodal distributions, it is necessary to postulate a hitherto unobserved state of ClO lying below the ground state ClO dissociation limit. The ground state configuration of ClO is $(\pi)^4(\pi^*)^3$, and the $A\ ^2\Pi$ state is the only possible molecular state excited by a $\pi^* \leftarrow \pi$ transition; however, in halogen compounds, the unoccupied σ^* orbital is relatively close in energy to the π^* orbital, and high spin states from a $\sigma^* \leftarrow \pi^*$ excitation are bound. For example, the lowest excited states of Cl_2 are the weakly bound $^3\Pi_J$ states arising from the $(\pi)^4(\pi^*)^3(\sigma^*)^1$ configuration. These metastable states lie ~7 kcal/mol below the Cl_2 dissociation limit. The existence of an analogous low lying state of ClO with configuration $(\pi)^4(\pi^*)^2(\sigma^*)^1$ is thus plausible, and would have $^4\Sigma$ symmetry. Langhoff has predicted the existence of a weakly bound $^4\Sigma^-$ state in unpublished *ab initio* calculations performed in the course of an earlier study of ClO doublet states.[21] In a recent recalculation, he estimates that this state, the $a\ ^4\Sigma^-$ state, has an energy T_0=51 kcal/mol above the ground state.

If the theoretical value of T_0 is correct, formation of ClO in the $a\ ^4\Sigma^-$ state is energetically allowed in photolysis of Cl_2O at both 308 and 248 nm. At 308 nm, the energy available for translation upon formation of ClO ($a\ ^4\Sigma^-$) is E_{avl}=9 kcal/mol, but essentially no products at these low translational energies were observed. At 248 nm, where E_{avl}=31 kcal/mol, the slower component in the 248 nm $P(E_T)$ distribution has a maximum at 21 kcal/mol and thus conceivably could be due to the channel

$$Cl_2O + h\nu \rightarrow ClO(a\ ^4\Sigma^-) + Cl(^2P). \quad (9)$$

These products can only correlate with a triplet state of Cl_2O. Such a state could be formed by a spin–orbit induced Landau–Zener transition occurring at the intersection of an initially prepared singlet surface and a repulsive triplet surface of Cl_2O.

B. The Cl_2+O channel

We have presented direct evidence for the concerted dissociation forming $Cl_2 + O(^3P)$ products following excitation at 193 nm. Over 80% of the Cl_2 products undergo spontaneous secondary dissociation in the collisionless conditions of our experiment; the Cl_2 products that do reach the detector appear to be highly excited, with 53 kcal/mol or more of internal energy. The positive anisotropy parameter indicates that the transition moment and recoil vectors are approximately parallel. Given that these vectors are perpendicular to the a axis of this near prolate top, the low value of β prevents us from reaching conclusions concerning the time scale of the dissociation.[14] These observations are consistent with a concerted mechanism occurring on a surface with an early exit barrier, in which the Cl–Cl bond would form while the chlorine atoms are still widely separated.

The high internal energy of the Cl_2 products could arise if the Cl_2 molecules are formed in an electronically excited state. The lowest excited states of Cl_2 are the A, A', and B states, which are the three J levels of the $^3\Pi$ configuration lying 49.1, 50.7, and 50.9 kcal/mol, respectively, above the ground state. Formation of chlorine in any of these states is energetically consistent with the data. Furthermore, the $Cl_2(^3\Pi) + O(^3P)$ channel would occur by a spin-allowed process upon initial excitation to a singlet state, whereas the ground state products $Cl_2(X\ ^1\Sigma) + O(^3P)$ would be formed via a spin-forbidden path. Production of triplet chlorine molecules thus provides the simplest explanation for the observed results. If this hypothesis is correct, prompt emission from Cl_2 should be observed following 193 nm photolysis of Cl_2O.

We did not observe the Cl_2+O channel when photolyzing at 308 or 248 nm, although it is energetically allowed at both wavelengths. A 193 nm photon excites Cl_2O in an entirely new band, and it is possible that the barrier for concerted elimination of Cl_2 is significantly lower on the new potential energy surface (*vide infra*).

A concerted dissociation channel has also been observed in the photolysis of OClO in the 300–400 nm region

$$OClO + h\nu \rightarrow Cl + O_2. \quad (10)$$

In contrast to our observations on Cl_2O, Davis and Lee[22] have found that the O_2 product from OClO appears to be formed with little internal energy, and O_2 may in fact be formed in the $^1\Delta_g$ state. The excited state is predissociative (the absorption spectrum is highly structured), and the angular distribution of photoproducts is isotropic, indicating that the excited molecule lives longer than a rotational period. These conclusions are supported by a recent time-resolved study by Baumert *et al.*[23] The dynamics of this concerted dissociation are thus considerably different from those in Cl_2O dissociation. The mechanism is believed to involve a nonadiabatic transition from the initially prepared state to a highly bent $^2B_2$ state.[24] The small bond angle at the minimum energy configuration of this surface favors formation of O_2. A similar coupling of electronic states may also be occurring in Cl_2O.

C. The 2Cl+O channel

We find evidence for complete dissociation of Cl_2O into three atoms upon excitation at 248 and 193 nm, but not at 308 nm which lies to the red of the 294 nm threshold. At 248 nm, this channel occurs by secondary dissociation of the primary ClO photofragments. Simple bond fission leading to ClO+Cl products dominates, and formation of $2Cl + O(^3P)$ products is a minor secondary channel. The $2Cl + O\ (^1D)$ can also occur at high laser fluences by stimulated secondary dissociation of ClO, because ClO has a large absorption cross section.

In contrast, at 193 nm, almost all of the primary Cl_2 photoproducts spontaneously dissociate. ClO that is detected is highly excited and it is probable that most of the primary ClO also undergoes secondary dissociation. Although we could not determine if concerted three body dissociation occurs upon photolysis at 193 nm, we can conclude that photolysis of Cl_2O at 193 nm leads predominantly to three atomic fragments in the absence of quenching collisions.

Our results are consistent with early photolysis experiments which found evidence for atomic oxygen photoproducts upon irradiation at wavelengths λ<294 nm. Our findings support Edgecomb *et al.*,[7] who hypothesized that a

limited yield of atomic oxygen is formed via the 2Cl+O channel in the 235–275 nm photolysis experiment of Schumacher and Townend.[5]

The quantum yield of 0.25 ± 0.05 for atomic oxygen found by Sander and Friedl[9] can also be understood qualitatively. Both channels (2) and (3) contribute to O atom formation because the wavelength range of the xenon flashlamp used to photolyze Cl_2O extends to 180 nm. At wavelengths just below threshold, but longer than 200 nm, 2Cl+O products are probably formed by the secondary dissociation of ClO products. Below 200 nm, additional atomic oxygen is formed by the Cl_2+O channel (3), but most of the Cl_2 also undergoes secondary dissociation. Channel (2) is thus effectively the dominant source of O atom photoproducts, with dissociation to three atomic fragments probably resulting from secondary dissociation of highly excited diatomic fragments. The relatively low O atom yield indicates that most of the photolysis occurs at longer wavelengths, a conclusion consistent with the intensity distribution of a xenon flashlamp which decreases rapidly for $\lambda<300$ nm. Another possible source of O atoms, stimulated secondary dissociation of the ClO products, was not discussed in their paper.

D. Electronic structure of Cl_2O

The photoelectron spectrum of Cl_2O reveals four low-lying molecular orbitals, all within 40 kcal/mol (1.7 eV) of the highest occupied molecular orbital (HOMO).[25] The orbitals have been assigned by *ab initio* calculations,[26,27] taking into account perturbation corrections to the Koopmans' theorem energies,[26] and all four contain significant Cl p character. The highest occupied orbitals in the ground state configuration of Cl_2O are $\cdots(8a_2)^2(9a_1)^2(2b_2)^2(3b_1)^2$. The lowest unoccupied molecular orbital (LUMO) is the $10a_1$ orbital, which possesses significant σ^*(ClO) character.

The orbitals are close in energy, and thus assignment of the absorption spectrum is possible only with the aid of calculations that treat electron correlation. Lee has computed energies of the first ten singlet excited states in an *ab initio* calculation using a coupled-clusters perturbation technique CCSD(T).[28] He finds five states below 130 kcal/mol all with predominantly single excitation character, including one $^1B_2$ state at 103 kcal/mol (276 nm). In a recent multireference configuration interaction calculation, Langhoff also finds a $^1B_2$ state at $\simeq$110 kcal/mol (280 nm) with a large transition moment to the ground state;[21] given the large uncertainties in the calculations, this state is a likely candidate for either the shoulder at 284 nm or the main band at 255 nm. Langhoff also predicts at least three other dark states, all triplets, below 200 nm. Kuwata *et al.* identify a high-lying $^1A_1$ state at $\sim$7 eV in a singles-and-doubles configuration interaction (CISD) calculation, and assign it to the absorption band at 171 nm.[29]

The emerging theoretical picture of the excited states of ClO, while incomplete, qualitatively supports a number of the inferences that we have drawn from the experimental results. If we are exciting to the $^1B_2$ state at 308 and 248 nm, the transition moment is perpendicular to the C_{2v} symmetry axis and approximately parallel to the c.m. recoil vector, consistent with the observed values of β. An electron excited from the b_2 orbital (weakly antibonding for ClO) to the LUMO [the σ^*(ClO) $10a_1$ orbital] should lead to ClO bond cleavage. The different dynamical pathways leading to the ClO+Cl products could be the result of nonadiabatic transitions from an initially prepared state to one of the many predicted dark states. Spin–orbit coupling to one of the triplet states would allow the formation of spin-forbidden products such as quartet ClO.

The transition moment for excitation to the predicted $^1A_1$ state at 6.8 eV is parallel to the symmetry axis, consistent with the anisotropy parameter measured for the Cl_2+O channel at 193 nm. Concerted dissociation leading to Cl_2 products is most favored on surfaces with the potential energy minimized at small ClOCl bond angles. Promotion of an electron from the b_2 orbital to the a_1 orbital will decrease this angle because the b_2 orbital is a formally antibonding orbital σ^* for the Cl–Cl bond, while the LUMO a_1 has $\sigma(Cl_2)$ bonding character. The doubly excited configuration that involves exciting both b_2 electrons into the a_1 orbital will have $^1A_1$ symmetry. In this configuration, two electrons are promoted from a σ^* (Cl_2) orbital into a $\sigma(Cl_2)$ bonding orbital; therefore, this $^1A_1$ state is expected to possess an even smaller bond angle than the $^1B_2$ state. Excitation at 193 nm to a $^1A_1$ state could prepare a state with significant admixture of the double b_2 excitation, or it could be followed by vibronic (Herzberg–Teller) coupling to a B_2 state; in either case, the potential energy surface would favor small bond angles and a lower barrier for concerted dissociation.

ACKNOWLEDGMENTS

This work was performed at the Jet Propulsion Laboratory, California Institute of Technology, under contract with the National Aeronautics and Space Administration (NASA), and was supported by the Caltech President's Fund, NASA contract NAS 7-918, National Science Foundation PYI Award CHE-8957243, and a Dreyfus Newly Appointed Faculty Award. C. M. N. acknowledges support of a NASA Graduate Research Fellowship. We thank Timothy Lee and Steven Langhoff for providing unpublished results.

[1] C. L. Lin, J. Chem. Eng. Data **21**, 411 (1976); L. T. Molina and M. J. Molina, J. Phys. Chem. **82**, 2410 (1978); H. D. Knauth, H. Alberti, and H. Clausen *ibid.* **83**, 1604 (1979).
[2] J. B. Nee, J. Quant. Spectrosc. Radiat. Transfer **46**, 55 (1991).
[3] W. Finkelnburg, H. J. Schumacher, and G. Stieger, Z. Phys. Chem. B **15**, 127 (1931).
[4] S. Abramowitz and M. W. Chase, Jr., Pure Appl. Chem. **63**, 1449 (1991); M. W. Chase, Jr., C. A. Davies, J. R. Downey, Jr., D. J. Frurip, R. A. McDonald, and A. N. Syverud, *JANAF Thermochemical Tables*, 3rd ed., J. Phys. Chem. Ref. Data **14**, Suppl. 1 (1985).
[5] H. J. Schumacher and R. V. Townend, Z. Phys. Chem. B **20**, 375 (1933).
[6] F. J. Lipscomb, R. G. W. Norrish, and B. A. Thrush, Proc. R. Soc. London Ser. A **233**, 455 (1956); G. G. Freeman and L. F. Phillips, J. Phys. Chem. **72**, 3025 (1968).
[7] F. H. C. Edgecomb, R. G. W. Norrish, F. R. S. Thrush, and B. A. Thrush, Proc. R. Soc London Ser. A **243**, 24 (1957).
[8] N. Basco and S. K. Dogra, Proc. R. Soc. London Ser. A **323**, 401 (1971).
[9] S. P. Sander and R. R. Friedl, J. Phys. Chem. **93**, 4764 (1989).
[10] T. K. Minton, C. M. Nelson, T. A. Moore, and M. Okumura, Science **258**, 1342 (1992).
[11] Y. T. Lee, J. D. McDonald, P. R. LeBreton, and D. R. Herschbach, Rev. Sci. Instrum. **40**, 1402 (1969); M. J. O'Laughlin, B. P. Reid, and R. K. Sparks, J. Chem. Phys. **83**, 5647 (1985).
[12] G. H. Cady, Inorg. Synth. **5**, 156 (1957).
[13] R. N. Zare, Mol. Photochem. **4**, 1 (1972).

[14] S.-C. Yang and R. Bersohn, J. Chem. Phys. **61**, 4400 (1974).
[15] R. K. Sparks, K. Shobatake, L. R. Carlson, and Y. T. Lee, J. Chem. Phys. **75**, 3838 (1981); P. Felder (private communication). The forward convolution program used was FRAGMENT.
[16] R. A. Durie and D. A. Ramsey, Can J. Phys. **36**, 35 (1958); H. F. Davis and Y. T. Lee (private communication).
[17] W. B. DeMore, S. P. Sander, D. M. Golden, R. F. Hampson, M. J. Kurylo, C. J. Howard, A. R. Ravishankara, C. E. Kolb, and M. J. Molina, Chemical Kinetics and Photochemical Data for Use in Stratospheric Modeling, Evaluation No. 10, Publication 92-20, Jet Propulsion Laboratory, 1992.
[18] K. P. Huber and G. Herzberg, *Constants of Diatomic Molecules* (Van Nostrand–Reinhold, New York, 1977).
[19] G. E. Busch and K. R. Wilson, J. Chem. Phys. **56**, 3626 (1972); A. F. Tuck, J. Chem. Soc. Faraday Trans. 2 **73**, 689 (1977); L. J. Butler, Ph.D thesis, University of California, Berkeley, 1985; C. S. Effenhauser, P. Felder, and J. R. Huber, J. Phys. Chem. **94**, 296 (1990).
[20] J. B. Nee and K. J. Hsu, in *Proceedings of the International Conference on Global and Regional Environmental Atmospheric Chemistry, Beijing, China, May 1989*, edited by L. Newman, W. Wang, and C. B. Xiang (Brookhaven National Laboratory, Upton, NY, 1990).
[21] S. R. Langhoff (private communication).
[22] H. F. Davis and Y. T. Lee, J. Phys. Chem. **96**, 5681 (1992).
[23] T. Baumert, J. L. Herek, and A. H. Zewail, J. Chem. Phys. **99**, 4430 (1993).
[24] K. A. Peterson and H.-J. Werner, J. Chem. Phys. **96**, 8948 (1992); J. L. Gole, J. Phys. Chem. **84**, 1333 (1980).
[25] A. B. Cornford, D. C. Frost, F. G. Herring, and C. A. McDowell, J. Chem. Phys. **55**, 2820 (1971).
[26] D. P. Chong, F. G. Herring, and Y. Takahata, J. Electron. Spectrosc. Relat. Phenom. **13**, 39 (1978).
[27] K. Takano, J. Hosoya, and S. Iwata, J. Am. Chem. Soc. **104**, 3998 (1982).
[28] T. J. Lee (private communication).
[29] K. Kuwata, W. A. Goddard, and M. Okumura (unpublished results).